J. Iran. Chem. Soc., Vol. 7, Suppl., July 2010, pp. S123-S129.

JOURNAL OF THE
Iranian
Chemical Society

Magnetism Study of $C^{I}_{x}Co_{y}[Fe(CN)_{6}]\cdot zH_{2}O$ (C^{I}=Rb,Cs) Prussian Blue Nanoparticles

J. F. Xu[a], H. Liu[a], P. Liu[a], C.H. Liang[a], Q. Wang[a], J. Fang[a], J.H. Zhao[a,*] and W.G. Shen[a,b]
[a]*Department of Chemistry, Lanzhou University, Lanzhou 730000*
[b]*Department of Chemistry, East China University of Science and Technology, Shanghai 200237*

(Received 25 October 2009, Accepted 18 February 2010)

We synthesized a series of cobalt-iron Prussian blue analogues in the form of nanocubes with which we tuned the amount of Cesium cation in the tetrahedral sites of the structure and varied nature of the alkali cation in the compound adopting a single microemulsion technique. Structure and morphology of the compound had been investigated by combining energy-dispersive X-ray spectroscopy (EDS), inductively coupled plasma (ICP), thermo-gravimetry analysis (TGA), infrared spectroscopy (IR), powder X-ray diffraction (XRD) and Transmission electron microscopy experiments (TEM). To directly determine the coercivity, remanence and Curie temperature, superconducting quantum interference device magnetometer (SQUID) was performed. Our investigation suggests that the amount and nature of the alkali cation are critical parameters for understanding the magnetic properties of the nanoparticles.

Keywords: Prussian blue analogues, Single microemulsion, Magnetic properties, Nanoparticles

INTRODUCTION

Prussian blue analogues are a group of important functional materials due to their special properties in electrocatalytic, [1-3] electrochromic, [4] ion sieving, [5,6] photomagnetic, [7-15] kinetic spectrophotometeric field [16] and so on. In 1996, Hashimoto and co-wokers first described that spectacular magnetization changes could be induced photochemically in a magnetic molecule-base Prussian blue analogue of $K_{0.2}Co_{1.4}Fe(CN)_{6}\cdot 6.9H_{2}O$. It was proposed that with the presence of diamagnetic low-spin Co^{III}-Fe^{II} pairs in the compound, electron transfer could be either thermally or photochemically initiated from Fe^{II} to Co^{III} through the cyanide bridge to produce Co^{II}-Fe^{III} magnetic pairs, which therefore led to dramatic changes in the magnetic and optical properties exhibited by the lattice. [7,17,18]

*Corresponding author. E-mail: zhaojihua@lzu.edu.cn

We have previously made research on the magnetic properties of KCoFePBA nanoparticles which are synthesized in CTAB microemulsion system. The results indicate that the presence of a certain amount CTAB in samples may be the reason for higher Curie temperature and coercivity ($K_{0.11}Co_{1.52}Fe(CN)_{6}Br_{0.09}CTA_{0.19}\cdot 4.89H_{2}O$, Tc = 20 K, Hc = 500 Oe). [19] In principle, tuning alkali metal cation content could lead to novel nanostructures with distinct magnetic properties. However, so far rather scant investigations on this subject have been reported. [20] Herein we exploited single microemulsion technique to effectively synthesize cobalt-iron PBA at nanoscale to address this issue. Microemulsion technique bears several striking advantages. As one type of "soft chemistry", the synthesis process is very easy to handle, requiring no special and expensive equipment necessary for experiments under extreme conditions. Furthermore, particle shape and size distributions can be readily controlled by adjusting a series of experimental parameters such as

temperature, surfactant types, additives, surfactant concentrations and mole ratios of water to surfactant. [21-23] Hence, tailoring nanoparticle geometry at will is feasible and desired functional nanomaterials can be conveniently obtained.

In this paper, a family of cobalt-iron Prussian blue analogues, $C^{I}_{x}Co_{y}[Fe(CN)_6]\cdot zH_2O$ (x = amount of alkali cation inserted per conventional cell, C^{I} = Cs，Rb) had been synthesized and characterized. In addition, the amount and nature of the alkali cation were varied to seek the appropriate parameters to synthesize novel PBAs with higher coercivity and Curie temperature. The results are crucial for understanding the properties of this family of compounds and are expected to provide useful insights into preparing new systems with improved magnetic properties.

EXPERIMENTAL

Materials and Sample Preparation

Sodium bis (2-ethylhexyl) sulfosuccinate, 96% (AOT, A.R.) was purchased from Aldrich, which was sliced up and dried in airer for two weeks. Cobalt chloride hexahydrate ($CoCl_2$•$6H_2O$, A.R.), potassium ferricyanide ($K_3[Fe(CN)_6]$, A.R.), Cesium chloride (CsCl, A.R.) and Rubidium chloride (RbCl, A.R.) were used as received from Tianjin Guangfu Fine Reagent Factory. Double distilled water was used throughout the experiments.

Nanoparticles of cobalt-iron cyanides were synthesized by single microemulsion technology as the following. 20 ml of 3.5562 g AOT/ isooctane and 0.45380 g 0.05 M $CoCl_2$ aqueous solution were mixed, vigorously stirred and maintained at 25 ℃ for 2 hours to obtain one transparent reverse micelle solutions. Thereafter, potassium ferricyanide and Cesium chloride / Rubidium chloride solution was added dropwise with a syringe pump to the transparent microemulsion and stirred. After 10 minutes, gray-brown opaque appeared and colored solid partially settled. The mixture was continuously stirred for 11 hours at 25 °C and deposited for 12 hours, and then the supernatant became completely clear and colorless. The precipitates were centrifuged and then washed several times with ethanol (99.5%) and 1:1 (V/V) mixture of ethanol and water to remove the contaminated oil, surfactant and other inorganic substance from the particles. Finally, the solid were dispersed in ethanol (99.5%) for transmission electron microscopy characterization.

Products with different Cesium content were synthesized by varying the concentrations of $CoCl_2$, $K_3[Fe(CN)_6]$ and CsCl/RbCl.

Instrumentation

Powder X-ray diffraction (XRD) data were collected on a Rigaku D/MAX-2400 X-ray diffractometer with graphite monochromatized Cu Kα radiation (λ=0.15406 nm). Transmission electron microscopy (TEM) was performed by use of a Hitachi H-600 at an accelerating voltage of 100 kV to examine the morphology and dimension of the cobalt-iron PBA nanoparticles. The infrared spectroscopy (IR) spectra were recorded on a NEXUS670 FTIR spectrometer with samples prepared as KBr pellets. The elemental analysis was obtained from the energy-dispersive X-ray spectroscopy (EDS) (JSM-5600LV, KEVEX), inductively coupled plasma (ICP) (IRIS ER/S, PHEMO), and thermo-gravimetry analysis (TGA) (Netzsch Sta 449C). Magnetic properties were investigated with a superconducting quantum interference device (SQUID) magnetometer (Quantum Design MPMS XL).

RESULTS AND DISCUSSION

Morphology Analysis

Ultrafine cobalt-iron cyanide particles were prepared by AOT single microemulsion method with varied concentration of reactants and a fixed *w* of 45, the water/surfactant ratio. All the as-synthesized products (named sample $1^{\#}$ to $4^{\#}$, respectively) are found to have similar morphologies of regular nanocubes and sizes about 50-60 nm. Hence, TEM image of compound $1^{\#}$ was demonstrated as one representative in Fig. 1. Table 1 lists the formulas of the four cobalt-iron PBA prepared samples under different conditions.

Structure and IR Analysis

The crystal structures of the products were determined by XRD measurement, and the typical diffraction pattern

Table 1. Formulas of cobalt-iron PBA prepared in different conditions

sample	T(°C)	$[CoCl_2]$: $[K_3Fe(CN)_6]$: [RbCl][a]/ [CsCl][a]	Formula[b]
1#	25	50:10:12	$Rb_{0.12}Co_{1.37}[Fe(CN)_6] \cdot 4.54H_2O$
2#	25	30: 20: 3	$Cs_{0.12}Co_{1.34}[Fe(CN)_6] \cdot 3.58H_2O$
3#	25	30:14:6	$Cs_{0.32}Co_{1.31}[Fe(CN)_6] \cdot 2.25H_2O$
4#	25	30:14:10	$Cs_{0.53}Co_{1.31}[Fe(CN)_6] \cdot 3.20H_2O$

a. $[CoCl_2]$, $[K_3Fe(CN)_6]$, [RbCl] and [CsCl] refer to actual reactant concentrations (unit: mmol•L^{-1}).

b. Determined by ICP, EDS, TGA analysis.

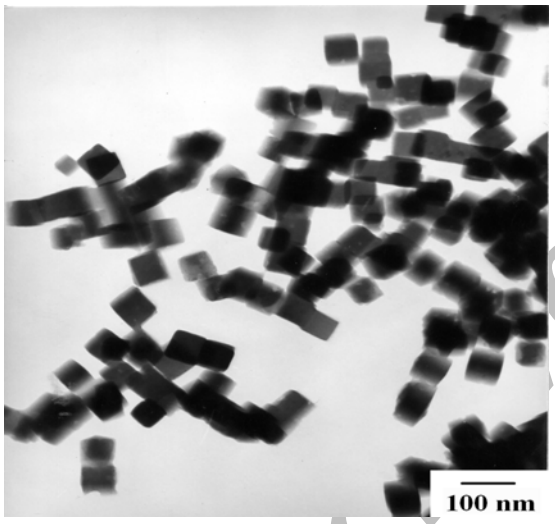

Fig. 1. Typical TEM images of cobalt-iron PBA

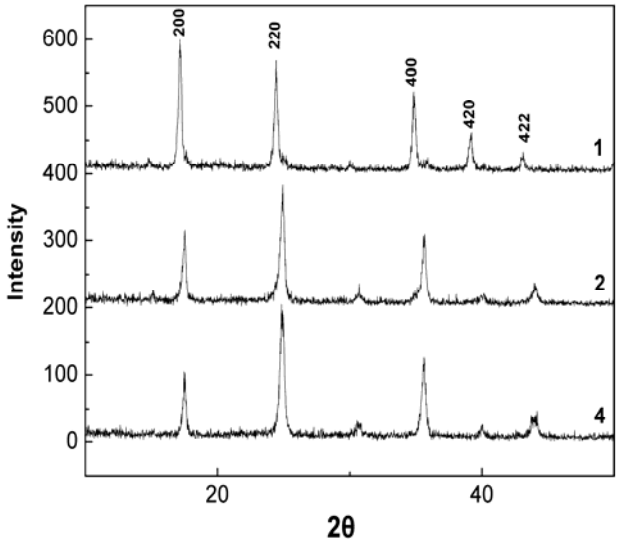

Fig. 2. XRD pattern of cobalt-iron PBA

(sample 1#, 2#and 4#) are shown in Fig. 2. The sharp intense peaks of 1# at 2θ values, 17.16°, 24.44°, 34.84°, 39.22°, 43.12°, which correspond to the {200}, {220}, {400}, {420} and {422} reflections, are readily indexed as a PBA face-centered-cubic (fcc) phase (JCPD card No.75-0038). [24] The other samples are all fcc phase, though there is an important difference between the XRD of 1# and those of samples 2# and 4#. Sample 1# with the rubidium cation contained is prone to grow along {200}, whereas the other sample 2#, 3#, 4# with the cesium cations grows along {220}, as indicated by the relatively more intense {200} reflection of the former. [25] The evidence firmly supports that different alkali ions result in varying growth direction of crystal. From the various indicators of diffraction peaks in Fig. 2, the lattice constant of 1# and 2# are calculated as 1.0295 nm and 1.0086 nm, respectively, by the use of least squares estimates. Considering that the Co^{II}-L bond is longer than the Co^{III}-L, more Co^{II} species are concluded to exist in compound 1#, grain of PBA doped with rubidium, than in compound 2# doped with cesium.

As for the FT-IR spectra of 1# to 4# at room temperature (Fig. 3), no characteristic band of surfactant AOT is detected in the spectra. ν_{OH} at 3631 cm^{-1} and 3400 cm^{-1} and 1607 cm^{-1}

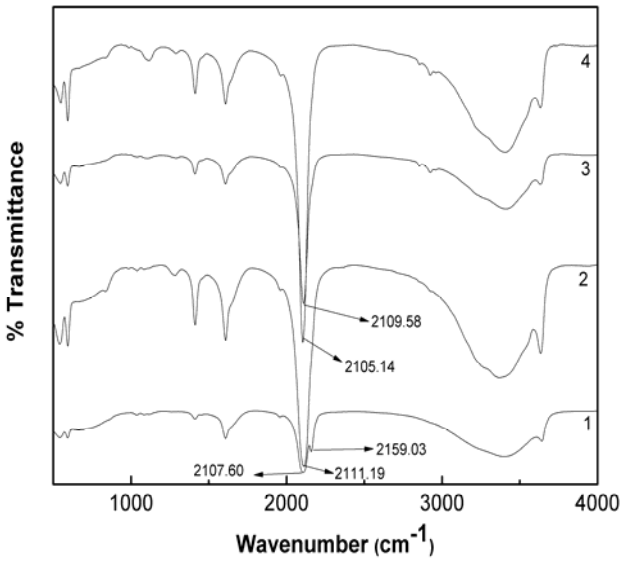

Fig. 3. Infrared (IR) spectra of cobalt-iron PBA of sample $1^{\#}$ to $4^{\#}$

are attributed to the stretching vibrations of liberating and associating of water to cobalt-iron PBA. [26] Over the cyanide vibration range, three bands are observed: the band at 2120 cm^{-1} is attributed to the cyanide in the Fe^{II}-CN-Co^{III} entities whereas the band at 2090 cm^{-1} is assigned to the cyanide in the Fe^{II}-CN-Co^{II} entities. [12] The band at 2159 cm^{-1}, exhibited as a shoulder peak only appeared for sample $1^{\#}$, is attributed to the cyanide stretching vibration mode in the Fe^{III}-CN-Co^{II} entities. The spectra of compounds $1^{\#}$ to $4^{\#}$ exhibit band centering at 2105-2111 cm^{-1}, envelope of the Fe^{II}-CN-Co^{III} and Fe^{II}-CN-Co^{II} contributions.

Magnetic Properties of the PBA Nanoparticles

Fig. 4a and Fig. 4b are the magnetic hysteresis loops at 5 K and magnetization curves at an external magnetic field of 5000 G for samples $1^{\#}$ to $4^{\#}$. The corresponding values of Curie, coercivity and remanence are calculated and summarized in Table 2. In the present paper, we tuned nature and the amount of inserted cations (Rb/Cs) to obtain different products. To minimize the interference of other factors, the nanoparticle size is limited to 50-60 nm and the cobalt-to-iron ratio is restricted in the range of 1.31-1.37.

The magnetic properties are getting weaker in the order of $2^{\#}\rightarrow 3^{\#}\rightarrow 4^{\#}$: coercivity decreased from 200 Oe to 0 Oe, the Curie temperature lowered from 18.2 K to 12.0 K and the remanence reduced from 0.9 emu/g to 0 emu/g. A possible reason for this may be illuminated as follows: The electron transfer is accompanied by a bond lengthening that has to be taken up by the inorganic network. With the cesium cation content increasing from 0 to 0.7 per cell, the average cell parameter increases and the Co-L bond becomes longer, because the insertion of the cesium cation leads to the decrease of the ligand field of $\triangle_{Co}$. However, from 0.7 to 4 cesium cations per cell, the average cell parameter progressively decreases, with a larger slope value between 0.9 and 2. [12] This variation reflects the progressive transformation of Co^{II} (HS) species to Co^{III} (LS) species in the structure and the corresponding average decrease of Co-L length [12]. In one unit cell, the number of divalent cations is always four so that the number of hexacyanometalate and alkali cations can be calculated. [11] In the order of $2^{\#}$ **(**0.36 cesium cations per cell**)**$\rightarrow$ $3^{\#}$(1.0 cesium cations per cell)$\rightarrow 4^{\#}$(1.6 cesium cations per cell), the Co-L bonds are getting shorter. Thus, Co^{II} species in the structure decrease along with the order of $2^{\#}\rightarrow 3^{\#}\rightarrow 4^{\#}$, which means the corresponding amount of Fe^{II}-CN-Co^{II} is reducing as well, and this structure reduction will result in the diminishing of magnetic property.

Moreover, for cobalt-iron PBA of $C^{I}_{x}Co_{y}[Fe(CN)_{6}]\cdot zH_{2}O$, with the enhancement of x, the negative charge of $[Fe(CN)_6]$ has to increase according in order to ensure the electroneutrality of the sample. Consequently, the solid vacancies decrease. As is well known, vacancy in solid blocks the magnetic domain mobility and magnetic moment reversal. Hence, the reducing of coercivity is accompanied by the decreasing of vacancy and the increase of cesium content in the range of 0.7 to 4 per cell as well.

To have a better understanding of the influence of different alkali cations on the inorganic network, we exploited rubidium as the alkali cation and synthesized sample $1^{\#}$ accordingly for comparison, with other parameters like the amount of alkali cation, cobalt-to-iron ratios and sizes being similar to those of sample $2^{\#}$. As can be seen from Table 2, H_c of $1^{\#}$ and $2^{\#}$ are same, but M_r of sample $1^{\#}$ is higher than that of $2^{\#}$. Presumably, this phenomenon is related to magnetic dipolar

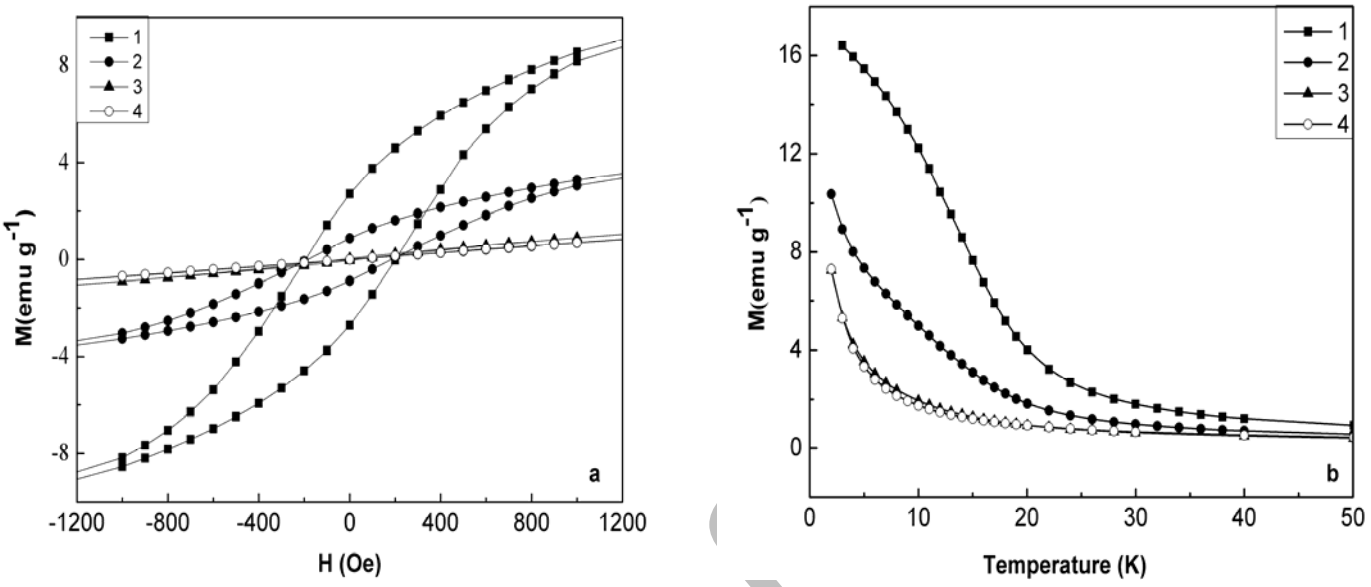

Fig. 4. Magnetic properties for $1^{\#}$ to $4^{\#}$ **;** (a) Hysteresis loops of samples $1^{\#}$ to $4^{\#}$ at 5 K; (b) Magnetization as a function of temperature at an external magnetic field of 5000 G

interaction and intergranular exchange coupling. For Prussian blue analogues, single domain magnetic particles of the saturation magnetization M_s is expressed as: $M_s \sim 2K_1/(H_c\mu_0)$, (μ_0, the permeability of vacuum; K_1, magnetic anisotropy constant), based on Stoner-Wohlfarth theory. [27] The relation reveals that the variation of M_s is proportional to that of K_1 when H_c is unchanged. Furthermore, it has been investigated that K_1 increases with the effect of grain increasing. For the PBA, it should be noted that its magnetic properties are largely determined by the electron spin and orbital coupling effect of the Fe-CN-Co. While the coupling effect of Co^{II}-L are larger than that of Co^{III}-L, larger amount of Co^{II}-L obtained for the rubidium-doped PBA than cesium-doped leads to higher K_1 and M_s. [28-30] As is well known, M_s is closely related with M_r, therefore the difference of M_r between $1^{\#}$ and $2^{\#}$ can be accounted for the difference of hydration ionic radius of alkali cation doped in PBA.

The magnetic properties of the compounds may, to some extent, depend on the nature of the alkali cation. First, the amount of inserted alkali cations was affected by the magnitude of the hydration ionic radius of alkali cation. [12] For example, among K, Rb and Cs, the hydration ionic radius of Cs is the smallest, so Cs^+ is easiest to be doped in the structure of PBA. Fewer cations contains the structure of lacunary type $A^{\square}_4[B^{\square}(CN)_6]_{8/3}$ and more vacancies, while more cations contains the structure of lacunary type $C^{\square}_4A^{\square}_4[B^{\square}(CN)_6]_4$ and fewer vacancies. [11] Second, the role of the alkali cation in the inorganic network, such as electrostatic effects, ion pairing, etc, is also depend on the nature of the alkali cation. [12]

CONCLUSION

In summary, we synthesized a series of cobalt-iron Prussian blue analogues in the form of nanocubes by using a single microemulsion technique. The nanoparticles were well-defined and uniformed in size within the range of 50-60 nm. The magnetic investigations on these products reveal that magnetism is dependent on the amount and nature of the alkali cation. In addition, as cobalt-iron cyanide with a Co/Fe ratio in the range 1.2-1.4 and the potassium contents are 0.2-0.6 can be optically excited, may shows that the efficiency of the

Table 2. Values of Curie temperature, coercivity and remanence at 5 K of samples 1# to 4#

sample	**1#**	**2#**	**3#**	**4#**
T_c (K)	19.0	18.2	12.0	12.0
H_c (Oe)	200	200	34	0
M_r(emu/g)	2.7	0.9	0.0	0.0

photoinduced magnetization at low temperature. Products prepared herein may also be promising candidates for applications in photomagnetic field.

ACKNOWLEDGMENTS

This work was supported by the National Natural Science Foundation of China (Projects 20473035, 20903051 and 20603014) and Committee of Science and Technology of Shanghai (Projects 0652nm010 and 08jc1408100).

REFERENCES

[1] M.H. Pournaghi-Azar, H. Dastangoo, Electrochim. Acta 48 (2003) 1797.
[2] D. Zhang, K. Wang, D.C. Sun, X.H. Xia, H.Y. Chen, Chem. Mater. 15 (2003) 4163.
[3] A. Eftekhari, J. Electroanal. Chem. 537 (2002) 59.
[4] K. Itaya, T. Ataka, S. Toshima, J. Am. Chem. Soc. 104 (1982) 4767.
[5] W.Q. Jin, A. Toutianoush, M. Pyrasch, J. Schnepf, H. Gottschalk, W. Rammensee, B. Tieke, J. Phys. Chem. B 107 (2003) 12062.
[6] M. Pyrasch, A. Toutianoush, W. Jin, J. Schnepf, B. Tieke, Chem. Mater. 15 (2003) 245.
[7] O. Sato, T. Iyoda, A. Fujishima, K. Hashimoto, Science 272 (1996) 704.
[8] O. Sato, Y. Einaga, T. Iyoda, A. Fujishima, K. Hashimoto, J. Phys. Chem. B 101 (1997) 3903.
[9] O. Sato, Y. Einaga, A. Fujishima, K. Hashimoto, Inorg. Chem. 38 (1999) 4405.
[10] N. Shimamoto, S.i. Ohkoshi, O. Sato, K. Hashimoto, Inorg. Chem. 41 (2002) 678.
[11] A. Bleuzen, C. Lomenech, V. Escax, F. Villain, F. Varret, C.C.d. Moulin, M. Verdaguer, J. Am. Chem. Soc. 122 (2000) 6648.
[12] V. Escax, A. Bleuzen, C.C.d. Moulin, F. Villain, A. Goujon, F. Varret, M. Verdaguer, J. Am. Chem. Soc. 123 (2001) 12536.
[13] J.H. Park, Y.D. Huh, E. Čižmár, S.G. Gamble, D.R. Talham, M.W. Meisel, J. Magn. Magn. Mater. 272-276 (2004) 1116.
[14] J.H. Park, E. Čižmár, M.W. Meisel, Y.D. Huh, F. Frye, S. Lane, D.R. Talham, Appl. Phys. Lett. 85 (2004) 3797.
[15] F.A. Frye, D.M. Pajerowski, S.M. Lane, N.E. Anderson, J.H. Park, M.W. Meisel, D.R. Talham, Polyhedron 26 (2007) 2281.
[16] B. Hemmateenejad, R. Miri, R. Kamali, J. Iran. Chem. Soc. 6 (2009) 113.
[17] M.Verdaguer, Science 272 (1996) 698.
[18] A. Bleuzen, C. Lomenech, A. Dolbecq, F. Villain, A. Goujon, O. Roubeau, Mol. Cryst. Liq. Cryst. 335 (1999) 253.
[19] H. Liu, X.L. Du, P.Y. Gao, J.H. Zhao, J. Fang, W.G. Shen, J. Magn. Magn. Mater. 322 (2010) 572.
[20] A. Bhattacharjee, S. Saha, S. Koner, V. Ksenofontov, S. Reimana, P. Gütlich, J. Magn. Magn. Mater. 302 (2006) 173.
[21] M. Yamada, T. Sato, M. Miyake, Y. Kobayashi, J. Colloid Interface Sci. 315 (2007) 369.
[22] S. Vaucher, M. Li, S. Mann, Angew. Chem. Int. Ed. 39 (2000) 1793.

[23] H.L. Sun, H.T. Shi, F. Zhao, L.M. Qi, S. Gao, Chem. Commun. 34 (2005) 4339.
[24] S. Choudhury, G.K. Dey, J.V. Yakhmi, J. Cryst. Growth 258 (2003) 197.
[25] X.B. Li, Y.G. Zhang, T.W. Li, Z.D. Zhang, Chem. Lett. 35 (2006) 506.
[26] L.H. Shi, T. Wu, M.J. Wang, D. Li, Y.J. Zhang, J.H. Li, Acta Chim. Sin. 23 (2005) 149.
[27] A.A. Sattar, H.M. El-sayed, K.M. El-shokrofy, M.M. El-tabey, J. Applied Sci. 5 (2005) 162.
[28] W.C. Feng, R.W. Gao, G.B. Han, J. Rare Earth 23 (2005) 52.
[29] H.P. Liang, Y.G. Guo, J.S. Hu, C.F. Zhu, L.J. Wan, C.L. Bai, Inorg. Chem. 44 (2005) 3013.
[30] J. Xiang, X.Q. Shen, Y.W. Zhu, J. Funct. Mater. 40 (2009) 365.